

Application of linear indexing model and GIS techniques for the slope movement susceptibility modeling in Bouselam upstream basin, Northeast Algeria

Riheb Hadji^{1,2} · Abdelmadjid Chouabi³ · Larbi Gadri⁴ · Khaled Raïs⁵ ·
Younes Hamed⁶ · Abderahmene Boumazbeur^{7,8}

Received: 16 May 2015 / Accepted: 18 September 2015 / Published online: 10 March 2016
© Saudi Society for Geosciences 2016

Abstract The main objective of this study was to assess spatial prediction of slopes movement susceptibility in the Bouselam upstream basin, northeast of Algeria, using a linear indexing model and Geographic Information Systems. First, the locations of 1109 slope instabilities, which occurred in the last three decades, were mapped upon data from various sources such as follows: remote sensing, aerial photographs interpretation, and internal reports compilation. This slope movement inventory was randomly segmented into training and validation datasets (75 % of the known events locations were used for training and building the model and the remaining 25 % for its validation). Second, nine natural and anthropogenic causing factors were mapped as independent variables: geological factors (lithology and faults density), morphometric

factors (slope, aspect, and elevations), environmental factors (precipitations, seism, and stream network density), and the land use factor (roads and rail network density). Third, the relative value of each categorical variable involved in the slope movements emergence was assessed (categorization of evaluation criteria, standardization of factors, and weighting of variables). Then, a global index value of slopes movement susceptibility was calculated for each cell in the study area by using a linear indexing model. Finally, the slopes movement susceptibility map was categorized into five hierarchic classes and validated using the validation dataset that was not used in the model building. The area under the curve was included to assess prediction capability of the adopted model (sensitivity=0.83 and 1-specificity=0.74). The resulted susceptibility map may be used for preliminary land planning purposes.

✉ Riheb Hadji
hadjirihab@yahoo.fr

¹ Department of Earth Sciences, Institute of Architecture and Earth Sciences, Ferhat Abbas Setif 1 University, Setif 19000, Algeria

² Laboratory of sedimentary environment, mineral and hydro resources, LESRMHAO, Tebessa University, Tebessa 12002, Algeria

³ Laboratory of Geodynamics and Natural Resources LGRN, Badji Mokhtar University, Annaba, Algeria

⁴ Mining Engineering Department and Mines Laboratory, Chieckh Larbi Tebessi University, Tebessa, Algeria

⁵ Electro-Mechanical Department, University of Skikda, Skikda, Algeria

⁶ Department of Earth Sciences, Faculty of Sciences, Gabes University, Gabes, Tunisia

⁷ Department of Earth Sciences, Faculty of Sciences, Tebessa University, Tebessa, Algeria

⁸ LESRMHAO Laboratory, Tebessa University, Tebessa, Algeria

Keywords Setif · Analytic-heuristic · Susceptibility · Natural breaks · Land use planning

Introduction

The Atlas chain NE Algeria is characterized by the recurrence of several types of slopes movement (SM), such as fall, topple, slide, spread, and flow. They result from the interaction of climatic, lithological, and morpho-structural conditions favorable to their course and could occur in a variety of materials and degrees of slopes (Djeral and Melbouci 2013; Guettouche 2013; Hadji et al. 2013a; Bourenane et al. 2014; Djeral et al. 2014). Most SM with recognized triggers are caused by rainfall and snow melt-water. In soils, the increase of pore-water pressures reduces shear resistance (Schumm et al. 2000; Phillips 2006). The occurrence of those SM is extremely damaging to

infrastructures and superstructures. In the wet years, there were recorded casualties. For example, in winter 2015, a rock fall occurred on the seaside of Aokas chief town on the RN°9 road that connects Setif to Bejaia, for the second time in the space of a few years, causing 7 people dead and 16 others gravely injured (Fig. 1). Two victims were reported in Medea Province after a mudslide and three people were killed in Tizi Ouzou Province because of a landslide, etc.

Setif Province is the second most populous department in Algeria and is considered the economic capital of Eastern Algeria; it holds significant socio-economic issues. Despite its importance, the slope movement susceptibility (SMS) is not taken into account in land planning of its territories. This research came to fill the breach due to the absence of regulatory tools to estimate and map the probability of occurrence of SM in this area.

The mapping of SMS depended on the quantity and quality of available data, the work scale, and the used approaches (Baeza and Corominas 2001). The analysis methodologies were divided between qualitative methods (direct type) and quantitative methods (indirect type) (Grozavu et al. 2013; Jaupaj et al. 2014). In respect of the direct type, a geomorphological qualitative zoning on the field was done to estimate the

SMS (Guzzetti 2005; Malet and Maquaire 2008), whereas indirect approach allows a quantitative allocation of hierarchical susceptibility levels (Akgun et al. 2012), it is often considered more objective by scientists. Other methods were probably applied to evaluate the susceptibility, including AHP (Park et al. 2013), WoE (Regmi et al. 2014), ANN (Youssef et al. 2010), Fuzzy Logic (Sharma et al. 2013), decision tree (Pradhan 2013), etc.

The used approach in this research was based upon a probabilistic empirical model, defining statistically the spatial relationship between the dependent factor (SM) and independent factors (predictive variables) (Anbalagan 1992). It proceeded through the following steps:

- (i) Detecting the SM from the images interpretation and their identification by field work;
- (ii) Mapping the causing factors of the SM occurrence in the study area;
- (iii) Analyzing the relative importance of each categorical variable involved in the SM emergence (categorization of evaluation criteria, standardization of categories, and weighting of factors);
- (iv) Assessing and mapping the SMS, and finally validating the model used in the modeling.



Fig. 1 The rock fall occurred February 24, 2015 at 13 h 30' near Aokas City on the RN°9 road connecting Setif to Bejaia

The number of parameters and categories involved in modeling depended on the spatial representativeness of attributes and on the evaluation of the expert who managed the study (Mastere et al. 2014).

The study area

The upstream Bousselam sub-watershed (code 15-06) covered an area of 1791.813 km² representing nearly 35 % of the total area of the main Bousselam watershed. This later belonged to Bousselam-Soummam major watershed, part of the great Algerois-Hodna-Soummam complex basin (Fig. 2a). The basin is located in the northeast of Algeria between 4°58'55.42" to 5°35'39.29"E longitudes and 35°45'03.01" to 36°20'53.22"N latitudes (Fig. 2b). It is surrounded by the Highlands Constantine watershed in the east, "Chott" El Hodna watershed in the south, the medium-Bousselam sub-watershed in the west, and Kebir Rhumel and Coastal-Constantine basins in the north.

The study area is bounded in the north by Jebel Medjounes, Jebel Aissel, Jebel Megriss, and Jebel Matrona; in the east by Kef Boudjemline, Jebel Merouane, Jebel Youssef, and Jebel Sekrine; and in the south by Jebel Hassane, Jebel Sattor, and Kef Della. The sub-watershed Bousselam upstream expands

over the western part of the Setif Province and intersects with five major sectors: Setif, Aïn Arnat, Aïn Oulmene, Guidjel, and Salah Bey as well as part of the east of Bordj Bou-Arreidj Province represented by Aïn Taghrout and Ras El Oued major sectors. This zone contains 15 municipalities: 11 in Setif and 4 in Bordj Bou-Arreidj.

The population of the study area reached 691,198 inhabitants with an annual growth rate of about 2.09 %. Setif Province includes 323,583 people or 46.81 % of the total population of the basin.

The agricultural activities in the basin are divided among mountain agriculture, apiculture, and tree farming in the north, in addition to extensive farming, cereal, fallow, and livestock (sheep, cattle, and poultry) in the center and south. The industrial activities concentrate around Setif and Aïn Oulmene cities. The main industries are agribusiness, wood, paper, leather, textiles, plastics, chemicals, glass, and metallurgy, besides mechanical engineering, electrical engineering, hydraulic engineering, quarrying, construction materials, public works, etc.

The climate of the study area is continental to semi-arid with two main seasons: rainy and cold from September to May, yet the second season is dry and hot during the remainder of the year. The annual average of rainfall varied between 550 mm in the north and 300 mm in the south (±200 mm). Analysis of weather data of the last four decades (1973–2013)

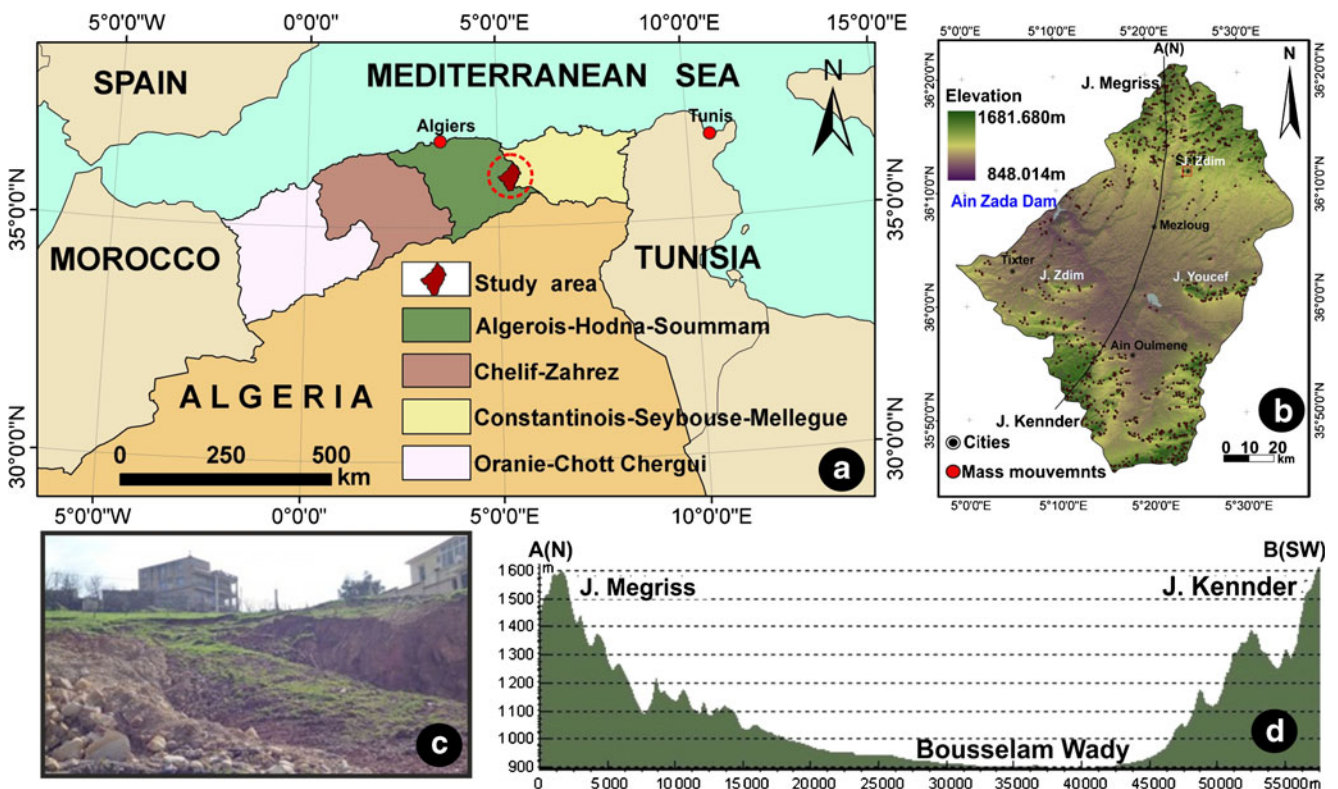


Fig. 2 a Geographical location of the study area in Algeria and Maghreb; b SM listed in the upstream Bousselam basin; c example of landslides that occurred in the study area; d N-SW topographic section between Jebel Megriss (a) and Jebel Kender (b)

(on the Essfiha ONM station, code 384) showed that the coldest month was January with an average of 5.38 °C, while the warmest month was July with 26.32 °C. The wettest month was December with an average of 48.95 mm while the driest was July with 12.83 mm. The rainy season (September to May) had 93 % of the annual precipitations specifying 69 days of rain. The mountain peaks were abundantly covered with snow during the winter, which helped trigger SM when it thawed in spring. SM, like that figured in (Fig. 2c), have become a common landscape inside and outside the cities.

The carbonate formations of the Lower and the Upper Cretaceous constitute the main aquifers in the study area. These aquifers constitute an important hydrogeological sequence in the Bousselam basin and host a significant shallow aquifer used extensively for both drinking and irrigation water.

The topography consisted of mountains chains, hills, and uplands (Fig. 2d). The average altitude of the basin was 1020.250 masl. Jebel Megris culminated at 1681.680 masl and Aïn Zada dam was the lowest point with 848.014 masl.

The Bousselam wadi is the major stream course in the study area (65 km). With a SW direction in upstream and NW direction in the center and downstream, it originated in the foothills of Jebel Megris and Jebel Aissel in the north and on the slopes of Jebel Sekrine in the south. Its main tributaries were Ftaissa wadi, Fermatou wadi, Khalfoun wadi, Tbinet wadi, Guellal wadi, Tixter wadi, Mellah wadi, etc. The drainage density was 3.03 km/km², which resulted in a slightly faster runoff, especially since the basin was characterized by a strong relief (250 m < Ds < 500 m). KC index was estimated at 1.15 indicating an elongate basin. The concentration time calculated by Giandotti formula (Thibault 2011) was Tc = 27.19 h.

Concerning the geological setting of the study area, there were five main structural sets: Numidian thrust sheets, Tellian thrust sheets, South-Setifian allochthonous set, South-Setifian autochthonous set, and anon-tectonic set. The main formations were the Eocene and Flysch formations at the upstream of the basin. The Mio-Plio-Quaternary deposits and Eocene material in the center and Hodanian coverage associated with an exotic extrusive Triassic in south. Twenty-eight carbonate formations outcropped in the study area (Fig. 3); their main components were as follows: limestone, marl, clay, sandstone, dolostone, and quaternary deposits with countless tuffaceous crusts. Fracture zones consisted of a variety of faults, thrust sheets, and overlap (Vila 1980).

Materials and methods

The used approach required the compilation of a set of cartographic information, alphanumeric data, aerial photos, and satellite images. All these documents were stored in the study geodatabase. A grid cell model was used for the spatial

modeling of layers. They were resampled at the same cell size and all data perfectly overlap. ESRI ArcGIS 9.3® (+ package) and XLStat-Pro7.5 software were broadly used for data processing. The SM inventory was taken from the visual interpretation of aerial photos and satellite images sequences. GPS (“Garmin GPSMAP 62” device) was used to track the position of the recognized events.

This study proposes the joint use of Geographic Information Systems (GIS) techniques and multi-criteria analysis to assess and map the SMS in the Bousselam upstream basin, following indirect heuristic method. This method allowed the estimation of the susceptibility, on the basis on the implementation of various parameters involved in the slopes rupture process (ordered in a GIS environment as georeferenced thematic layers). Their relative contribution to the phenomenon occurrence was formulated by assigning weights interpreting the proven role in the field. The weighting procedure was based on statistical data obtained from the analysis of the overlaid relationship between the spatial distribution of SM events (dependent variable) and each causative factor (independent variable) involved in the sliding process. After the individual allocation of corresponding weight (W_i) to each information layer, susceptibility elementary indexes (S_{ij}) were assigned independently to any class within each information layer, so that the total number of events occurring in each class was normalized with respect to its surface. After the indexing and the standardization procedure, all maps were rasterized into a 10 × 10 m grid. For each information layer (i), its weight (W_i) was multiplied by the elementary susceptibility index (S_{ij}) of any class (j). All information layers (from $i=1$ ton) were then combined with a linear summation in a global susceptibility index (IS) map using the Eq. (1):

$$IS = \left\{ f(x) \cdot \left(\sum_{i=1}^n [W_i \cdot S_{ij}(x)] \right) \right\} \quad (1)$$

With

- IS Global susceptibility index
- $f(x)$ Filter function depending on the slope angle (β) when $\beta \leq 3^\circ$, then $f(x) = 0$
- n Parameters number: i , parameter order; j , class order
- W_i Weight assigned to the parameter i (information layer)
- S_{ij} Elementary susceptibility index of the class (j) in the layer information (i).

To validate the predictive system, the interrelation between sensitivity (the occurrence of events) and specificity (the global susceptibility index) of the test was verified for all used values using a receiver operating characteristic (ROC) curve (Chung and Fabbri 1999). The area under the ROC curve (AUC) defined the model quality by characterizing its capability to predict the occurrence or the non-occurrence of a specific event. If its value exceeds 0.80, it will indicate a good model quality (Abul Hasanat et al. 2010).

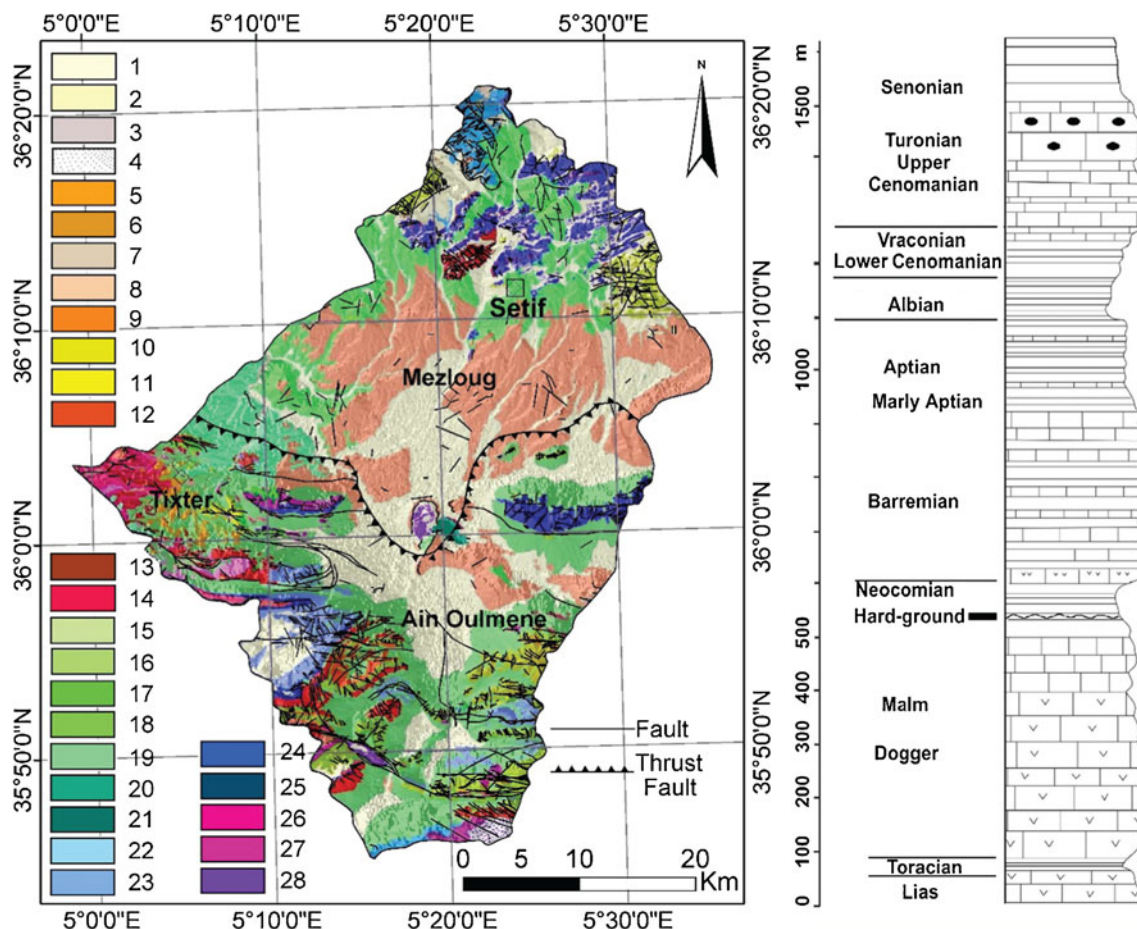


Fig. 3 a The geological map of the study area; b the stratigraphic column of the study area. Legend of the geological map: 1—recent alluvium, 2—slope unconsolidated formations, 3—topsoil, 4—slopes scree, 5—limestone with flints, 6—blackish marl, 7—brown and yellow limestone marl, 8—Bandy clays, 9—yellowish marl, 10—redhead sandstone and conglomerates, 11—sandstones, 12—sandy loam, 13—marly and limestone tiles, 14—yellow-

marl, 15—dolostone, 16—black marl, 17—marl and limestone sub-lithographic, 18—dolostone and limestone with flints, 19—gray marl and limestone, 20—marl and limestone, 21—limestone, 22—clay and sandstone benches, 23—marly limestone tiles, 24—phosphatic white limestone, 25—dolostones, 26—black marl, 27—varicoloured clays and ground gypsum, 28—fine limestone with saccocommides

The methodological chart of the adopted approach is shown in Fig. 4.

Data acquisition

The SMS modeling necessitates the processing of nine variables of ground parameters gathered from different sources. They were divided into geological, morphometric, environmental, and land use parameters. The information is derived from the digitization of existing geologic and topographic maps, the visual interpretation of aerial photographs and satellite imageries, the statistical treatment of rainfall amounts, the interpolation of seismic records and field surveys, etc. The data are computerized in different formats, as it is shown in Table 1.

Topographic data

Concerning the Digital Elevation Model (DEM) generation, a contour line map was digitized from an existing topographic

background in WGS84 UTM 31N projection and at 1:25,000 scale, with a contour interval of 10 m. A total of 247,627 altitude points were extracted from this contour line map. DEM (at 10×10 m resolution) was created upon these points and supported with 9972 GPS measuring points using the Inverse Distance Weighted (IDW) interpolation method. This DEM was the subject of various treatments (filling, resampling, etc.) in order to improve its resolution and visual quality.

Geological parameters

Lithology Lithology was digitalized from a background composed of six geological maps on 1:50,000 scale (Setif Number 93; Ain Azel, 143; Mezloug, 117; El Eulma, 94; Bir El Ahrech, 118; and Ain Taghrout, 116). Twenty-eight geological formations from the Trias to the actual were identified in the study area. According to their geotechnical and geomorphological characteristics, they were grouped into four

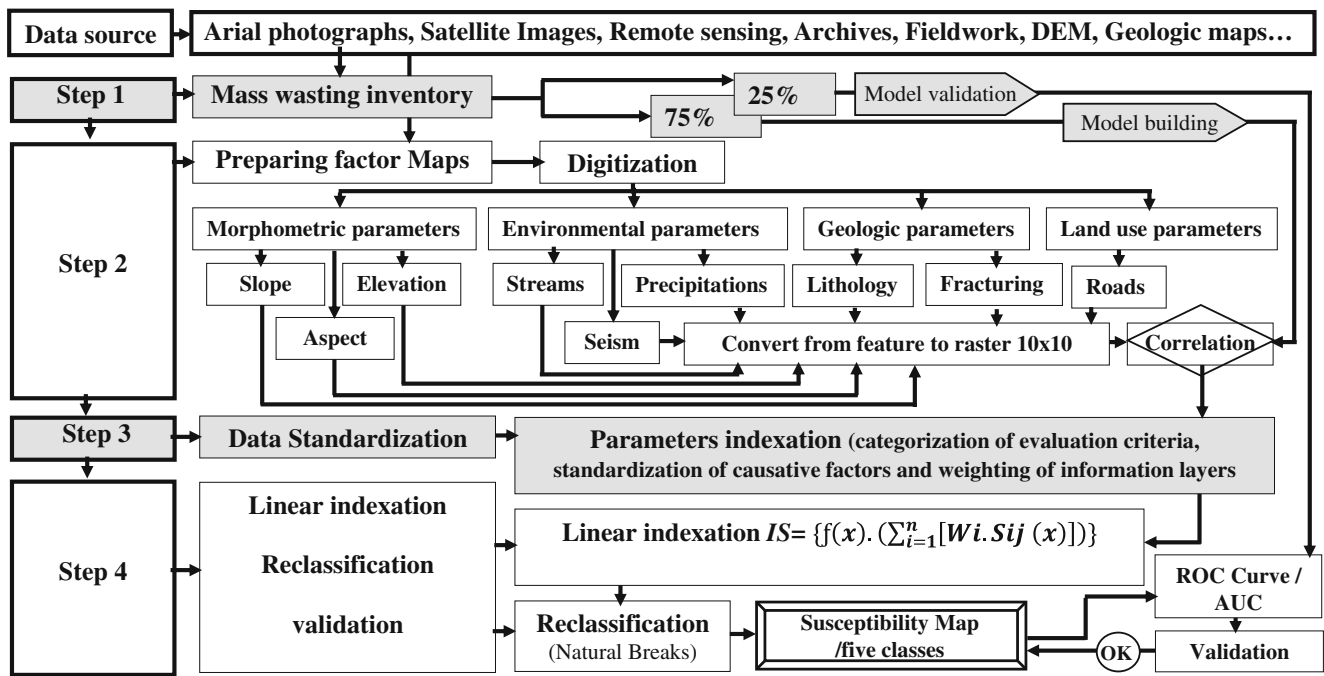


Fig. 4 The methodological chart of the adopted approach in the study

lithological units with an increasing susceptibility via the phenomenon: $UL_1, UL_2, UL_3,$ and UL_4 (Fig. 5a).

Faults density Tectonic discontinuities are known for their weakening effect on the resistance of geological formations (Mastere 2011). A faults map was digitized on the same six background assembly maps. It was updated by the integration of lineaments features detected from river system

anomalies and morpho-structural analysis. Recent bibliographic data were also added on the fault map (Harbi et al. 2003; Domzig 2006). This map served as a basis of the faults density map modeling (Fig. 5b). It included the cumulative lengths of the faults per unit of surface and illustrated the existence of tectonic nodes resulted from faults intersection. Fracture density was higher in the vicinity of thrust sheets fronts.

Table 1 Input data used in the for susceptibility assessment

Variables	Layer parameter	Data sources	Acquisition method	Data format
Topographic	DEM	Digitization and interpolation of elevation lines from topo (1:25,000) maps + GPS sampling	Georeferencing + digitization + interpolation	Raster
SM	SM inventory map	Aerial photographs and Landsat Satellite images visu-interpretation, field survey, documents analysis	Aerial photograph interpretation + field survey	Vector
Morphometric	Slope map	DEM	Derived from DEM	Raster
	Elevation map	DEM	Derived from DEM	Raster
	Aspect map	DEM	Derived from DEM	Raster
Geologic	Lithological map	Analysis of geological maps (1:50,000), geomorphological maps (1:200,000)	Interpretation of geological maps + field survey	Vector
	Fault density map	Aerial photographs, field survey, bibliographic data, topo maps	River system anomalies aerial photograph	Vector
Environmental	Stream density	Aerial photo, topo maps, DEM.	Automatic generation	Vector
	Precipitations	Precipitations records	Simple kriging	Vector
	Seism	Historical seismic data	Multi-step interpolation	Vector
Land use	Roads density	Satellite imagery, aerial photographs topo maps (1:25,000), field surveys, roads map	Remote sensors, georeferencing, digitization, interpolation	Vector

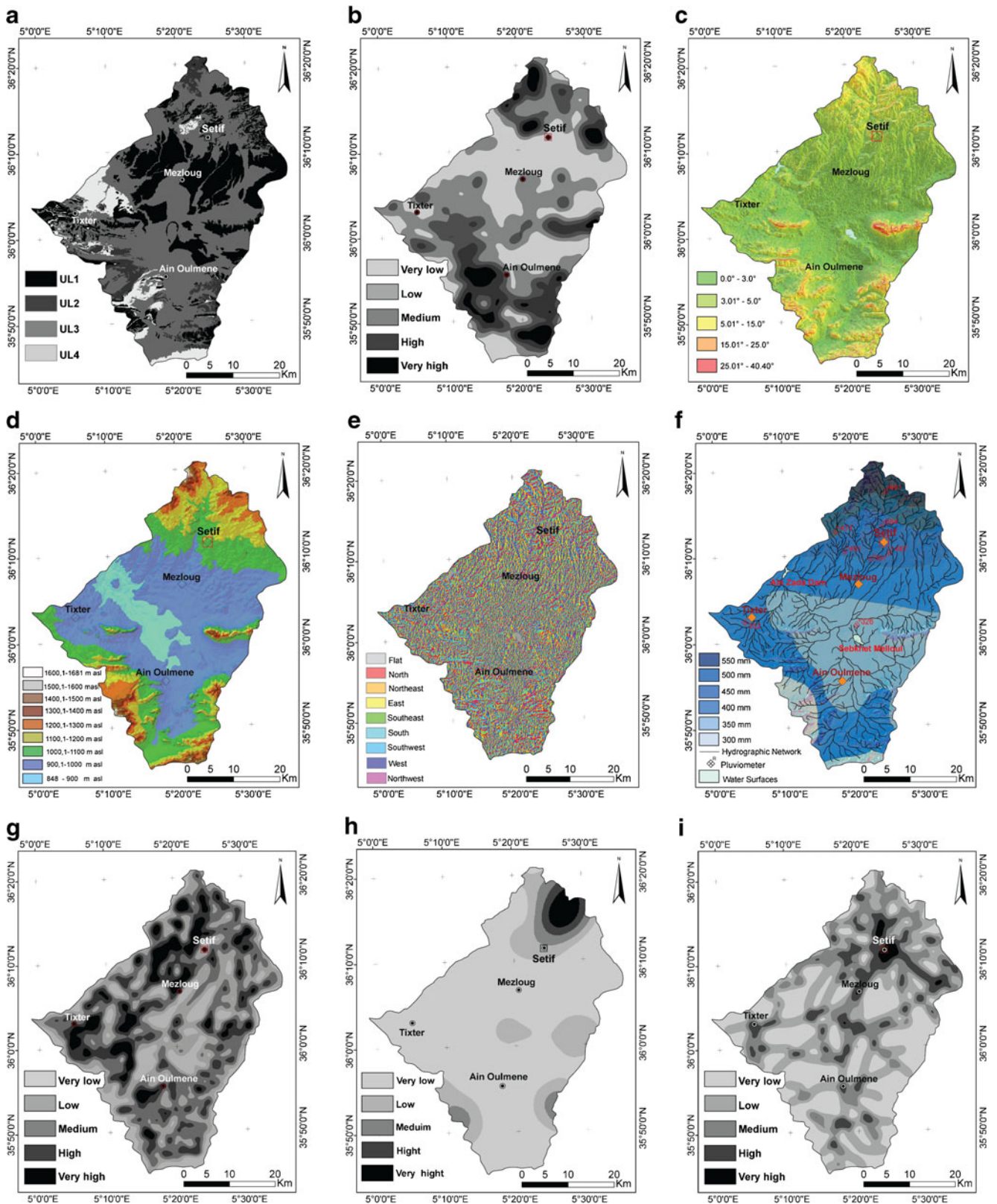


Fig. 5 a Lithological units (UL) outcropped in the study area. b The faults density map of the study area. c Slope classes map of the study area. d The elevation map of the study area. e The aspect map of the study area. f The precipitations interpolation map obtained by ordinary kriging

for September 1973 to August 2013 in the study area. g The stream system density map of the study area. h Seismic map (magnitudes) of the study area (with 1365–2009 period). i The road and rail network density map of the study area

Morphometric parameters

DEM allows extraction of the various morphometric parameters that would be combined in the study model (e.g., slope classes, relief amplitude, slope aspect, etc.).

Slope classes The slope gradient is the main causative factor to SM (Kundu et al. 2013). The average slope of the study area was about 5.53° with a standard deviation of 4.93° (Fig. 5c). Upon field observations, the slope map was divided into five classes: $\leq 3^\circ$, $[3^\circ, 5^\circ]$, $[5^\circ, 15^\circ]$, $[15^\circ, 25^\circ]$, and $>25^\circ$. In the first class $[0, 3^\circ]$, scarce events were recorded. The second class was not favorable to the development of the slopes movements. It corresponded to superficial debris flows. The coincidence of the third class with marl clayey formations showed a significant rise of the phenomenon. From the fourth class, events started to become apparent.

Relief amplitude The elevations map of the study area was divided into nine hypsometric classes ranked between 848 and 1681 masl (Fig. 5d). The $[1600, 1681\text{ m}]$ slice represented the highest elevation of the basin and correspond to the smallest class, with only 0.035 % of the entire study area. It is located on the summit of Jebel Megriss in the north and in Jebel Kennder in the southwest. The $[900, 1000\text{ m}]$ class is the largest class in size with 47.90 % of the basin area. The average elevation is 1020.260 m; it belonged to the $[1000, 1100\text{ m}]$ class, which covered 22.93 % of the expanded study area. The lowest area was $[848, 900\text{ m}]$; it covered the center of the study area with only 7.12 % of the total basin area. It was composed mainly of alluvial terraces.

Slope aspect The slopes aspect map expressed the relative exposure of slopes towards the north, following the clockwise direction. It revealed the most exposed slopes to solar radiation, and hence to evapotranspiration (Pourghasemi et al. 2012). The aspect map of the study area was also derived from the DEM (Fig. 5e). Winter rainfall disturbances came mainly from the northwest. The “Sirocco” hot winds from the southwest; they mutated the clay formations to their drawal limits (Hadji et al. 2014).

Environmental parameters

Environmental parameters could lead to the triggering of SM. The slope equilibrium can likely be disturbed by the rushing and draining water in the river courses and as well as seismic loading. Unfortunately, the combinations of rainfall intensity, rainfall duration, hydraulic conductivity, and antecedent moisture conditions are very difficult to map and require an enormous number of data (Ohlmacher and Davis 2003).

Precipitations Associated with the water courses system, precipitations are the main triggering factor of SM (Conforti et al. 2011). The spatiotemporal correlation between the SM occurrence and precipitations amount showed that the origin of instabilities was more related to the recurrence of severe disruption (as cloudbursts) than to rainfall usually spread over the same rainy season. This confirmed that the SM in the study region were especially water-controlled (Hadji 2013b). The analysis of temperature-precipitations series in Setif Province showed perceptible climatic disturbing changes over the past four decades. A first wet period stood up to 1986. A severe drought then settled for nearly 15 years from 1987 to 2002. It was followed by a return of a wet period since 2003. This return of rainfall was accompanied with an increasing of severe cloudburst disturbances (we mention severe cloudburst disturbance when precipitations exceed 30 mm per 24 h).

To estimate the spatial variability of precipitations over a 480-month monitoring period from September 1973 to August 2013, of 12 meteorological stations surrounding the study area, a simple kriging with varying local means (SKlm, Distances) was used to incorporate two types of exhaustive secondary information: (i) elevation extracted from a smoothed DEM and (ii) distance to a regional maximum rainfall (Goovaerts 2010; Mair and Fares 2010).

The resulting precipitations interpolation map included six classes: 300 mm isohyet class (4.71 %) covering the far south of the study area; 350 mm isohyet class (32.30 %) covering the center of the study area; 400 mm isohyet class (40.10 %) surrounding the last isohyet; 450 mm isohyet class (13.03 %) where the chief town of the province is located; 500 mm isohyet class (5.67 %) in the north; and 550 mm isohyet class (4.19 %) in the far north of the basin (Fig. 5f).

Drainage density Runoff carries an intermittent mechanism in SM triggering in mountainous areas (Park et al. 2013). The erosive potential of water in river systems and the hydrodynamic force of the current are quite influential factors in the initiation of new instabilities or the reactivation of old ones. By crossing the friable lithological formations, runoff generated large areas of ravines. The hydrographic network map was automatically produced from the DEM by exploiting the module ArcHydro Tools 9 in ArcMap. It was the basis of the production of the drainage density map, which included five hierarchical classes ranging from very low to very high (Fig. 5g).

Seismicity A part of SM is an induced phenomenon by earthquakes (Pareek et al. 2010). These seismic solicitations could reduce the soil consistency, amplify rock fracturing, and increase pore pressures in slopes. The seismicity of the study area was associated with the seismotectonic sources of the faults of Beni Ouartilene, Kherrata, Jebel Youssef, Jebel Tella, Djemila, and Guergour-Anini faults system (Harbi et al. 1999;

Bouhadad et al. 2003; Bouhadad 2008). Based on historical seismic data of the region (from 1365 to 2009) and using a multi-step interpolation, we mapped the potential of seismic sources in the study area. The expected maximum magnitudes were estimated by using the relation of Wells and Copper-smith (1994). Their recursion was considered using the truncated exponential recurrence model of Cornell and Van Marke (1969). For the attenuation model, the law of Sadigh was used (1993). The resulting map had five classes: very high ($M_s > 4.5$), high ($4.5 > M_s \geq 4.0$), medium ($4.0 > M_s \geq 3.5$), low ($3.5 > M_s \geq 3.0$), and very low ($M_s < 3.0$) (Fig. 5h).

Land use parameters

The road network was selected as the most influential anthropogenic factor in SM phenomenon apparition in the study area. This land use theme was designed using a multi-source database composed of Landsat 8 images, Northern Algeria roads map, and topographic maps (in 1:25,000 scale), confirmed by fieldwork. This map was the basis for generating the road network density map (Fig. 5i).

Analysis of the SM data

According to Varnes (1978), “Understanding the occurrence of past and present land movements is the key to the spatial prediction of this hazard in the future.” This essential step for any spatial modeling of the phenomenon required the compilation of a multi-temporal SM inventory as points feature in the GIS software. The inventory map includes the entire individual or multiple events in a given area during a given period (1984–2014). This data set was used to consider the quantitative relationship between the occurrence of the SM and their causative factors.

A total of 1109 SM that occurred during the last three decades was identified and projected in the inventory map (only events with a volume $\geq 25\text{m}^3$ were taken into account). The smallest inventoried SM was 25m^2 , and the largest one covered an area of $170,250\text{m}^2$ while the average size of all SM was 3460m^2 . All SM covered an area of 50.171km^2 or approximately 2.8 % of the overall surface area within the region. Upon the classification of Varnes (1984), four main types of SM were recognized:

- Rotational, planar, and compound landslides;
- Undermining superficial landslides initiated by rivers erosion and soil’s degradation;
- Debris flows;
- Rock falls.

They spread between 87 % of landslides: almost 8 % of rock falls, 3 % debris flows, and less than 2 % of the remaining varieties. We also encountered other types of gravitational

movements but with very minimal representation; they were neglected from the modeling. Nearly 75 % of the recognized SM (888 events) was used for the model construction and 25 % (221 events) for its validation. These were chosen randomly.

Several studies have proven the relationship of the occurrence of SM with predisposing and triggering factors (Zhou et al. 2002; Pradhan and Lee 2010; Mastere et al. 2011; Hadji et al. 2012; Guadri et al. 2015). Nine causative factors were retained for this study; these were as follows: two geological factors (lithology and faults density), three morphometric factors (slope, elevation and aspect), three environmental factors (precipitations, drainage density and earthquakes), and one land use factor related to roads density. Climatic and geomorphologic factors explained the occurrence of certain types of SM in this area. Debris flows in the northeast were significant to the prolonged action of meteoric water on unconsolidated formations. Rock falling in south and northwest was caused by the limestone fracturing in slopes above 30° . Rotational landslides in marl, silts, and clay formations were strongly influenced by the relief. Planar landslides are visible when soft formations overlay stratigraphic joints or a tectonic bedrock, etc.

All of SM inventoried in the study area were obtained using the air photo-interpretation, Landsat imagery sensing, morphological maps, and historical data completed by systematic field surveys. The SM were mapped in the field using a cartographic GPS with 1 m accuracy.

The SM boundaries were categorized into two areas: (i) a SM initiation zone and (ii) a SM accumulation zone (Thiery et al. 2007). This leads to build a GIS geodatabase containing information of the damages, frequencies, geometries, types, distribution, structures, depths, age, and state of activity of these instabilities.

The study considered any parameter showing a higher density of events than the overall density of SM in the study area (density $\geq 0.62\text{events/km}^2$) as an influential parameter.

For the three causative factors with linear character, buffer zones (multi-buffer) were created around the axes of roads, streams, and faults.

The analysis of the SM positions over road and rail networks (with multi-buffer of [0, 25], [25, 50], [50, 100], and $>100\text{m}$) showed that in areas $\leq 25\text{m}$ from road axes, the density was high (1.135events/km^2); it presented almost double compared to the class [25, 50 m] (0.526events/km^2). Beyond 50 m, density became low (0.479 and 0.457events/km^2) (Fig. 6a).

The analysis of the SM positions in relation to the river system (with a multi-buffer of [0, 25], [25, 50], [50, 100], and $>100\text{m}$) shows that in areas $\leq 25\text{m}$ from streams axes, the density is high (0.968events/km^2). The density became moderate in the [25, 50 m] class of (0.622events/km^2); beyond 50 m, the density turned into low (0.477 and

0.430 events/km²). This factor was less influential than the previous factor. This was probably due to intermittent seasonal characteristic of the flow in these rivers compared to the maintained traffic throughout the year on the roads in the study area (Fig. 6b).

The analysis of the SM positions with respect to faults (with multi-buffer of [0, 100], [100, 250], [250, 500], and >500 m) showed that in areas ≤100 m from lineaments, faults density was very high (2.216 events/km²). In the [100, 250 m] class, density was high (1.430 events/km²); beyond 250 m, the density becomes low (0.461 and 0.073 events/km²). This factor (in the nearest buffer <100 m) was more influential than road and stream network. This was probably due to the microseismic nature of these faults and that they constituted a moisture source to the overlying formations (Fig. 6c).

The correlation between these three factors with the listed SM positions showed an inverse correlation (more than the distance from roads, streams, and faults increases, the SM density decreases).

The analysis of the SM positions relative to the lithological units showed that the clayey-marl formations (UL₄) were the most affected units by the events with high density (1.442 events/km²). For the unit (UL₃) moderately susceptible to SM, the density was low (0.453 events/km²); in the remaining two classes (UL₂, UL₁), density was very low with (0.373 and 0.324 events/km²), respectively (Fig. 6d).

The analysis of the SM positions relative to precipitations isohyets showed that the wettest terrains (550 mm) were the most affected by the phenomenon with a high density in the order of (1.8 events/km²). This density gradually decreased with the decreasing of precipitations. However, the 300-mm class constituted the exception with an abnormal increase in the events density (0.947 events/km²). This was probably due to the action of another factor (eventually geomorphologic) on this part of the study area (Fig. 6e).

The superposition of the SM positions on slopes classes showed that the class of acute gradients [25°, 40°] corresponded to a very high density, with (3.561 events/km²) followed by the less-steep class [15–25°] with (2.228 events/km²) then [5–15°] with (1.839 events/km²), etc. (Fig. 6f). These results confirmed our field measurements which showed that SM were much related to this morphometric factor.

The analysis of the slopes aspect factor showed that the northwest, west, and north classes contained the largest concentration of SM with densities in the range of 1.067, 1.036, and 0.99 events/km², respectively. This was likely caused by the rain-showers action of northwestern cloudbursts (Fig. 6g).

The distribution of SM versus to altitude classes illustrated that [1500, 1600 m] and [1400, 1500 m] altitudes were the most affected elevations by the phenomenon with high densities (2.957 and 2.814 events/km², respectively). This was clearly due to the severe weather conditions (snow cover) and to the accumulation of weakly consolidated deposits resulting from

Fig. 6 **a** Density of SM relative to the road network density. **b** Density of SM relative to the drainage network density. **c** Density of SM relative to the faults density. **d** Density of SM relative to relative to the lithological units. **e** Density of SM relative to precipitations isohyets. **f** Density of SM relative to relative to the slope classes. **g** Density of SM relative to relative to the slopes aspect. **h** Density of SM relative to elevation classes. **i** Density of SM relative to seismic magnitudes

erosion on these altitudes. The [1600, 1681 m] classes recorded none event, this was due to the correspondence of these mountain peaks with massive rocky outcrops. Events were very rare in the lower classes near the watershed outlet. This was apparently due to the very low inclines of these lands (Fig. 6h).

The analysis of the SM spatial distribution relative to seismic factor showed that the events density grows around the expected higher magnitudes sectors ($M_s \geq 4.5$) (2.756 events/km²), followed by the [4.5, 4.0] class, with 2.657 events/km². The remaining classes had low densities. This was probably caused by the action of the steeper vibratory stresses near seismic sources such as active faults and thrust sheets (Fig. 6i).

The correlation between factors related to lithology, rainfall, slopes, hypsometry exposure, and earthquakes with the position of the listed SM indicated a normal correlation.

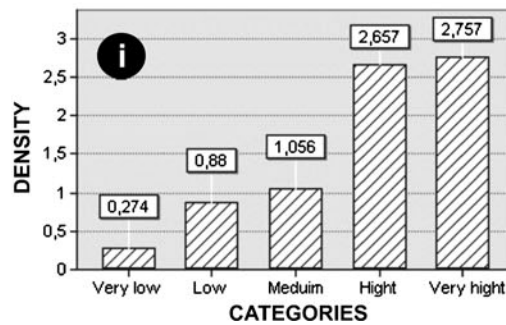
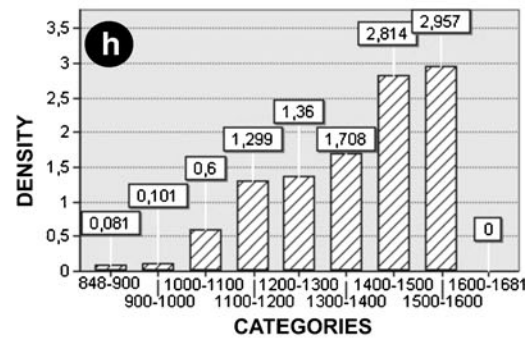
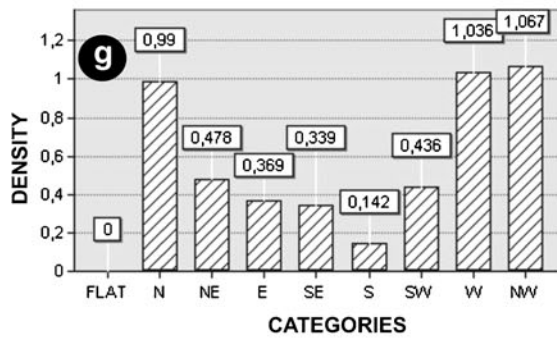
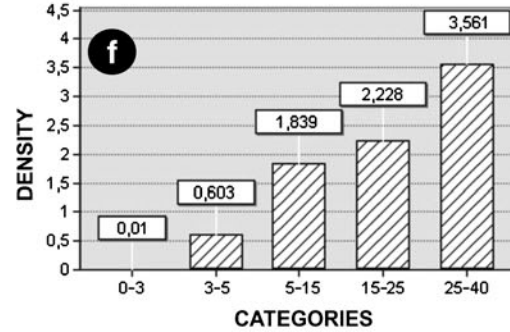
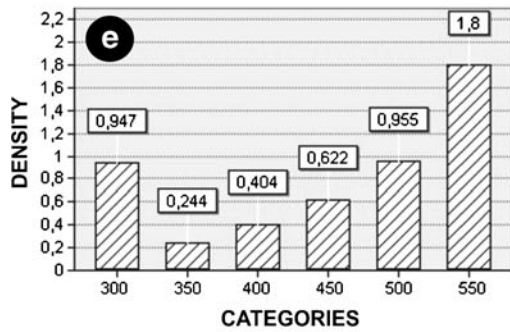
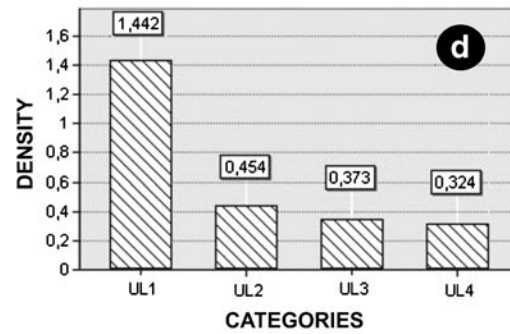
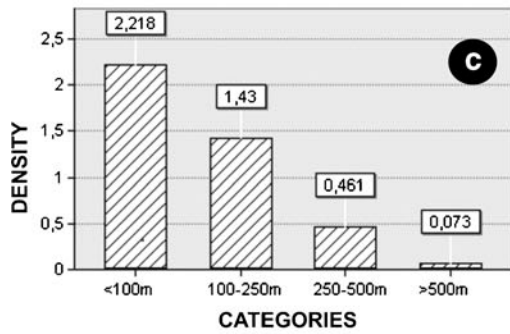
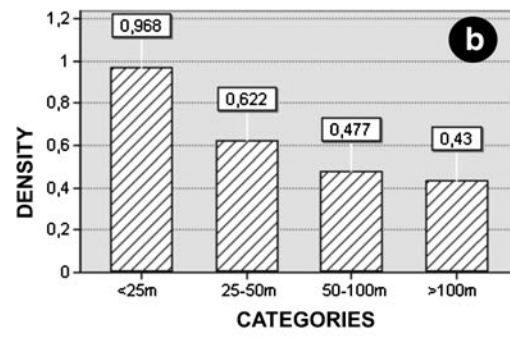
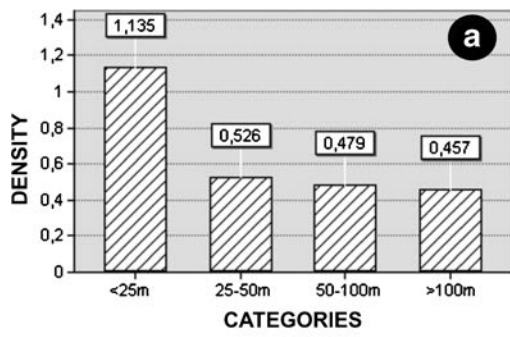
The application of the geomorphic threshold concept provides plausible explanations for some landforms. It allows the prediction of the unstable landscapes evolution in the study area. Geomorphic systems are typically nonlinear, due largely to their threshold-dominated nature (Schumm 1991). These dynamics make geographical and historical investigation unavoidable. Schumm (1979) established a hypothetical direct proportionality between valley-floor gradient and instability with time.

This research manages intrinsic and extrinsic geomorphic thresholds. The most determinants factors incorporated in the representation of our geomorphic system are slopes, hydrologic network, and erosion. The critical conditions of SM happening are attained when slopes exceed 15°. The depositional-steepening of valley floors causes the development of gullies. Consequently, failure occurs by gullying. This characteristic type of intrinsic threshold is the result of slope change throughout time. The geological and environmental parameters (as climatic or tectonic changes), soft formations, and seismic behavior are also eminent critical conditions in the change of landscapes response.

MM susceptibility zoning

After the rasterization of all factor maps in (10×10 m) grid cells, weighting procedure was undertaken for all selected causative factors (Pourghasemi et al. 2013). This task consisted of the following:

- The attribution of a weight value (W_i) (integer between 1 and 9) to each factor (i), reflecting its contribution in the



SM genesis. These values were determined quantitatively on the basis of the relationship between the spatial occurrence of events and the selected predictive variable. The most influential factor had to have a maximum value equal to 9;

- The allocation of an elementary susceptibility index (S_{ij}) (integer between 1 and 10) for each class (j) within each information layer (i). These values were determined on the basis of the relationship between the spatial distribution of the events and the selected elementary class surface.

Morphometric factors (especially the slope gradient) were drastically influential in the origination of SM in the study area. Values of 9 and 7 were assigned respectively to the slope and hypsometry parameters.

A maximum value of 9 was assigned to the lithology parameter because a considerable amount of SM was recorded on the clayey marl formations more susceptible to slope instabilities. Besides, geoscientific literature considered it as a major factor in the genesis of the phenomenon (Parise and Jibson 2000; Lee and Choi 2003). A value of 8 was attributed to the fracturing parameter because the prevalent SM were recorded where faults were denser. The same value of 8 was also been attributed to precipitations. A value of 7 was attributed to drainage and road density parameters. The same value (7) was attributed to seismic factor supported by the seismotectonic nature of abnormal contact. A minimum value of 4 was assigned to slope exposure as the least influential parameter in the SM occurrence.

Details of densities, frequencies, susceptibility indexes, and weights values of each factor and class influencing the SM emergence in the study area are shown in Table 2.

For modeling the SMS map of the study area, the contribution of all triggering factors was expressed as the sum of the arithmetic multiplication of the weights of different parameters (W_i) by the elementary susceptibility indexes of classes (S_{ij}) in each information layer. Applying Eq. (1) for the 17, 919,955 cells (with 5543 columns and 6702 rows) lead to get values of global susceptibility indexes “IS” comprised between 77 and 457 (Fig. 7). To facilitate the map interpretation, the continuous values (IS) were prioritized into five qualitative classes more comprehensible to the user (Akgun 2012; Demir et al. 2014).

ROC curves were tested (through the integration of 221 (25 %) events excluded from the modeling by a random process) for several mathematical clustering methods, such as equal intervals, defined intervals, geometrical interval, standard deviation, quintile classifications, etc. (Ayalew et al. 2004). The Natural Breaks classifier method gave a model with the highest positive (AUC) than the other methods (showing a sensitivity=0.83 and 1-specificity=0.74; deemed quite satisfactory). It was selected for correctly classifying pixels in the training dataset of the basin SMS map (Fig. 8a).

Results and discussion

In applying the linear indexing model, an efficient statistical processing is important. In addition to zonal statistics functions (within the main GIS packages), an external statistical program was used for the analysis. As discussed above, the relative importance of independent variables can be expressed by the empirical frequency ratios that reveals the most responsible causal factors in the occurrence of SM. Frequency ratios related to the lithology classes identify the UL₄ unit as particularly prone to landslide occurrences (FR=3.56). The variation follows a polynomial trend of second degree with a coefficient of determination ($R^2=0.95$). The slope gradient factor indicates a very well frequency values and emphasizes a direct proportionality between the increase of the slope angle and SM occurrence. Larger (FR=7.182) is calculated for angles steeper than 25°. The variation follows also a polynomial trend of second degree, with a coefficient of determination ($R^2=0.98$). SM have occurred where precipitations reach 550 mm with (FR=3.631). The variation follows a polynomial trend of second degree with a coefficient of determination ($R^2=0.94$). Most of the SM are controlled by seism magnitude ($M_s > 4.5$) with (FR=5.591). The elevation exhibit greater frequency (FR=5.963) when the values approach 1500–1600 masl, whereas for higher and lower classes the proportionality declines. However, we have to approach the third degree to reach a coefficient of determination ($R^2=0.80$). The more important statistical results showing relationship among variables are summarized in Table 3.

The calculated SMS map has a continuous scale of numerical values which need to be separated into susceptibility classes. We reclassified this map into five qualitative classes (from very low to very high) (Fig. 8c). The very low susceptibility class (index “IS” values ranges between 77 and 158) represented approximately 17.09 % of the total basin area. It covered plains and alluvial terraces. The individualization of this class was in perfect compliance with field observations (as it was characterized by the scarcity of SM). Building, networks, and activities do not take SMS into account. The low susceptibility class (IS values between 159 and 204) with 27.47 % of the entire study area represented the terrains bordering the previous class. It was located in the center of the basin occupied by more or less indurate formations. This zone corresponded to the faintly vegetated areas with low rainfall. The low susceptibility of this part of the basin was apparent due to its relatively gentle slopes. Building, networks, and activities need only consider SM as a minor threat. The moderate susceptibility class (value between 205 and 247) covered 28.55 % of the basin. It is situated in the north and in the south of the study area, near mountainous reliefs and in the fronts of overthrust sheets which delineated between Djemila allochthone and the South-Setifian autochthone.

Table 2 The spatial relationship between each causative factor and MM listed in the study area (parameters weighting, classes indexing, frequencies, and densities calculation)

Factor (<i>i</i>)		Class			SM		Density	Frequency	Index
<i>i</i>	W_i	<i>j</i>	Area (km ²)	%	Number	%	<i>D</i>	FR	(S_{ij})
Lithology	9	UL ₁	567.337	31.40	184	20.72	0.324	0.660	2
		UL ₂	158.259	6.32	59	6.64	0.373	1.050	3
		UL ₃	901.696	54.81	409	46.06	0.453	0.840	4
		UL ₄	163.707	7.47	236	26.58	1.442	3.560	10
Faults density	8	V. low	1220.277	68.13	104	11.71	0.085	0.172	0
		Low	289.783	16.18	189	21.28	0.652	1.315	2
		Moderate	141.534	7.90	191	21.50	1.349	2.722	4
		High	98.704	5.51	269	30.29	2.725	5.496	8
		V. high	40.701	2.27	135	15.22	3.317	6.689	10
Slopes (°)	9	[00–03°]	1078.013	60.19	11	1.23	0.010	0.021	0
		[03–05°]	416.055	23.23	251	28.27	0.603	1.217	2
		[05–15°]	184.858	10.32	340	38.29	1.839	3.710	5
		[15–25°]	64.834	4.74	189	21.28	2.228	4.493	6
		[25–40°]	27.239	1.52	97	10.93	3.561	7.182	10
Elevations (m)	7	[848–900]	148.367	8.28	12	1.35	0.081	0.163	0
		[900–1000]	849.687	47.44	86	9.68	0.101	0.204	0
		[1000–1100]	401.335	22.41	241	27.14	0.600	1.211	2
		[1100–1200]	231.644	12.93	301	33.89	1.299	2.621	4
		[1200–1300]	113.208	6.32	154	17.34	1.360	2.744	4
		[1300–1400]	32.782	1.83	56	6.31	1.708	3.445	6
		[1400–1500]	10.306	0.57	29	3.26	2.613	5.675	10
		[1500–1600]	3.044	0.17	9	1.03	2.957	5.963	10
Aspect	4	[1600–1681]	0.623	0.03	0	0	0	0	0
		Flat	27.033	1.51	0	0	0	0	0
		N	257.939	6.93	123	13.86	0.477	1.997	4
		NE	198.897	11.10	95	10.69	0.478	0.963	4
		E	184.233	10.29	68	7.66	0.369	0.744	3
		SE	206.744	11.54	70	7.88	0.338	0.683	3
		S	317.751	17.74	45	5.07	0.141	0.286	1
		SW	231.693	12.94	101	11.37	0.436	0.879	4
Precipitations (mm)	8	W	174.648	9.75	181	20.39	1.036	2.090	10
		NW	192.059	10.72	205	23.08	1.067	2.153	10
		300	84.489	4.72	80	9.01	0.947	1.909	2
		350	578.791	32.31	141	15.87	0.243	0.491	1
		400	717.846	40.08	290	32.66	0.403	0.815	2
		450	233.278	13.02	145	16.33	0.621	1.253	4
Streams density	7	500	101.612	5.67	97	10.92	0.954	1.925	5
		550	74.982	4.18	135	15.21	1.800	3.631	10
		V. low	259.456	14.48	115	12.95	0.443	0.894	8
		Low	463.663	25.89	220	24.78	0.474	0.957	8
		Moderate	571.098	31.89	281	31.64	0.492	0.992	9
Seism	7	High	337.779	18.86	181	20.38	0.536	1.081	9
		V. high	159.002	8.87	91	10.25	0.572	1.154	10
		V. Low	1374	76.74	377	42.45	0.274	0.553	1
		Low	274	15.30	241	27.14	0.879	1.773	3
		Moderate	71	3.96	75	8.45	1.056	2.132	4

Table 2 (continued)

Factor (<i>i</i>)	W_i	Class			SM		Density <i>D</i>	Frequency FR	Index (S_{ij})
		<i>j</i>	Area (km ²)	%	Number	%			
Road density	7	High	35	1.94	93	10.47	2.657	5.388	9
		V. high	37	2.05	102	11.49	2.756	5.591	10
		V. low	597.009	33.334	257	28.94	0.430	0.868	4
		Low	583.339	32.571	285	32.09	0.489	0.985	4
		Moderate	408.786	22.824	271	24.44	0.531	1.071	5
		High	181.469	10.132	106	11.94	0.584	1.178	5
		V. high	20.396	1.139	23	2.59	1.128	2.274	10

It is characterized by a combination of soft features, moderate slopes, and higher rainfall than the previous two classes. The reunion of these conditions made these areas moderately susceptible to SM. SMS should be considered when planning a development, but do not need to be a restrictive concern, except where the proposed activity exposes human life to the SM threat. The high susceptibility class (value between 248 and 300) covered 18.68 % of the total study area. It was located on the mountains foothills (especially in the north and south of the study area) and coincided with the elevations where there were more events. It was characterized by steep slopes often covered with snow in winters. Building should be restricted though safe sites should be identified in which mitigative procedures must be designed by a specialist. The very high susceptibility class (index range 301 and 457) covered 08.21 % of the basin. In this area, the faults density, slopes, and precipitations were very important, whereas the land cover is divided into poorly maintained forests and barren land. Geological formations were represented by fragile units on slopes exceeding 15°. This class was therefore more involved in triggering SM. Building should be prohibited; besides, people should be notified of the SMS and encouraged to take mitigation procedures (Saunders and Glassey 2007; England 2011). The results are also shown in tabular form in Table 4 and in diagrammatic form in Fig. 8b.

The distribution of these classes was in perfect consonance with the field observations since the environmental and anthropogenic conditions of each class predisposed differently these areas to the triggering of SM.

According to the produced results, the SM in the study area are mainly controlled by the lithology, slope gradient, and faults density predisposition factors, which agrees with the findings of other researchers elsewhere (Kamp et al. 2008), and as triggering factor by precipitations and quakes. A strong correlation between lithology and SM occurrence was obtained (with a maximum weight assigned to this parameter $W=9$). The phenomenon is mainly controlled by this factor. The comparison between the precipitations and SM show also a good correlations (with a weight $W=8$), which is similar for the

seismic factor with ($W=7$). These two last parameters trigger SM over the study area.

SMS assessment is more factual if it is related to an extreme rainfall event. SM activity reaches its maximum during and just after rainy events. During 2003, annual precipitations attained the extreme value of 587.5 mm in the middle of the study area and exceeded 870 mm in the north. Hundreds of SM of various types and sizes have been triggered. Data of SM frequency and precipitations pattern (1973–2013/Essfiha station, ONM code 384) were plotted in the same graph. It shows a close relationship between monthly precipitation and SM occurrence. An interannual comparison between the two

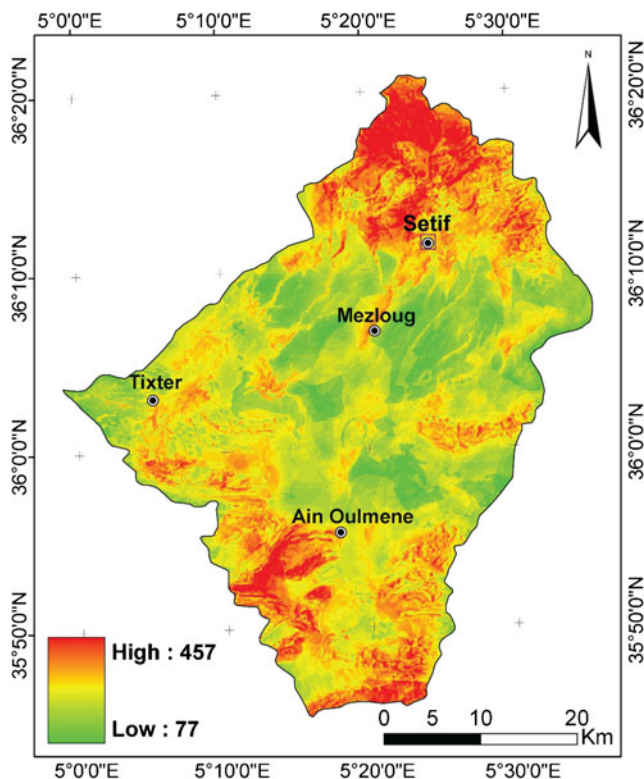


Fig. 7 The global susceptibility indexes map of the study area

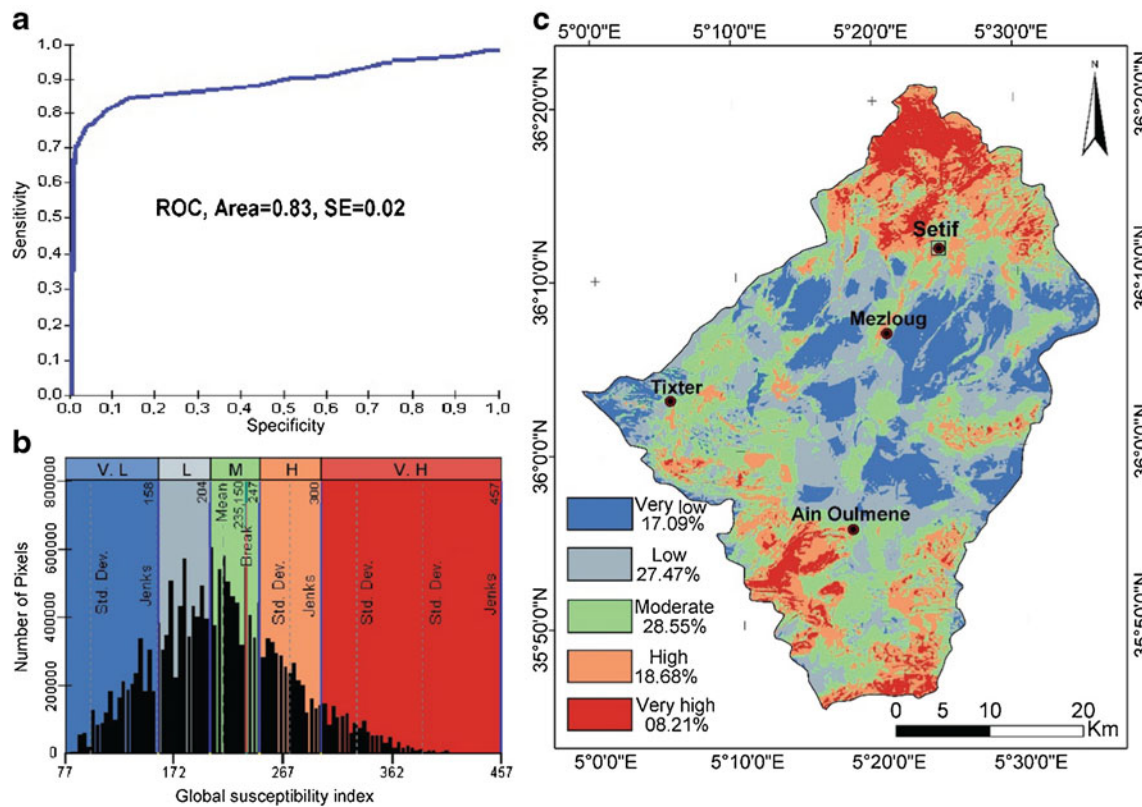


Fig. 8 a The ROC Curve of the adopted model. b The classification of the SMS histogram to a qualitative classes by Natural Breaks method. c The SMS map of Bousselam upstream basin

phenomena shows a return period of almost 5 to 6 years. Rainfall intensity, its duration, and hydraulic and moisture conditions control the water-level circulation on clayey marl and colluvium slopes (Haneberg and Gokce 1994).

The density (D) and the susceptibility index (S_{ij}) for UL₄ unit is significantly high. This means that “clays, marls, silty clays and colluvium formations” have a high susceptibility to the phenomenon occurrence that is not significantly different only from the slope value. The accumulation areas of large debris flows often show different size of scraps. On steep slopes, the soils seem to be a result of the substratum alteration; such material remains weak. Shallow landslides were observed on this milieu. Bedrock is not often affected, except

by rock falls especially if it is much fractured and when slope angles approach the vertical.

The probability of earthquake-induced mass wasting was taken into account in this study, which strengthens the validity of the resulting susceptibility assessment. There is a greater likelihood of seismic triggering of SM during the wet season in the study area. The favored SM typologies triggered by earthquakes could differ substantially from those triggered during rainfall events (Jibson 1996; Pallás et al. 2004). Some SM observed in the study area could have been triggered by seismic events rather than by rainfall. This could be the case of SM that do not necessarily involve large amounts of water such as earth flows and rockfalls.

Table 3 Statistical analysis results of most significative variables

	Min	Max	Mean	Std dev	Trend curve	R^2
Susceptibility	77	457	214.836	57.660	$Y = 0.17x^2 - 0.52x + 0.42$	0.98
Lithological units	1	4	2.383	1.007	$Y = 0.23x^2 - 1.52x + 2.68$	0.95
Precipitations (mm)	300	550	407.143	90.351	$Y = 0.15x^2 - 0.84x + 1.54$	0.94
Seism (deg. rich.)	2.8	4.3	2.912	0.295	$Y = 0.03x^2 + 0.50x - 0.29$	0.91
Slope (°)	00	40.4	5.53	4.93	$Y = 0.04x^2 + 0.6x - 0.65$	0.98
Elevation (masl)	848	1681	1020.26	115.46	$Y = 0.04x^3 + 0.58x^2 + 1.74x + 1.47$	0.80
Aspect	-1.0	360	179.55	103.88	$Y = 0.17x^3 + 1.24x^2 + 3.39x - 2.26$	0.78

Table 4 Qualitative meanings of SMS quantitative indices values

Quantitative values	Qualitative class	SM No	Area km ²	SM/km ²	Signification
77 to 158	Very low	2	306.221	0.006	Absence of SM
159 to 204	Low	76	492.211	0.154	SM occur infrequently and will be small and easily managed
205 to 247	Moderate	212	511.562	0.414	SM occur infrequently, but on rare occasions may be large enough to cause property damage
248 to 300	High	290	334.711	0.866	Damaging SM occur occasionally and smaller landslides may be frequent
301 to 457	Very high	308	147.108	2.094	Damaging SM are common

Conclusion, recommendations, and outlook perspectives

To evaluate the distribution of SMS over the study area, this research uses a statistical analysis, based on a probabilistic empirical model, with particular reference to SM events and physical parameters which are regarded to be significant in the SM occurrence.

The SMS map is considered as an end product that can be useful for land use planning and for the success of the development strategies in the study area, in order to avoid residing in potentially threatened sites by the studied hazards. The SM inventory in the study area revealed various types of slides ranging from simple superficial debris flows to large complex landslides. These geomorphologic phenomena were significantly influenced by unfavorable climatic conditions. The analysis of the number of severe weather events over the past 30 years showed a constant evolution. The share of stormy days in all of rainy days was increasingly growing. A relationship existed between changes in daily maximum temperatures and the number of storm days.

Our study offered a comprehensive research for spatial estimation of slope stability with an analytical-heuristic approach. Nine parameters involved in the SM occurrence were incorporated in the modeling. These were slope, lithology, faults density, and precipitations, which were assigned a maximum weight (9, 9, 8, and 8, respectively), as these parameters were the most influential factors in causing the SM in the study area. The drainage density, road network, earthquakes, and hypsometry were of weight (7) each, while the slopes aspect was the least influential factor, with a value of (4).

The importance of each class was quantitatively defined with a statistical process of the overlapping relationship between the spatial distributions of events in different parameters classes. The linear summation of the indexed maps gave a global quantitative indexes map (with SI ranging between 77 and 457). The “Natural Breaks” method was selected for the rescaling of the susceptibility map in five qualitative classes: very low susceptibility class (17.09 %), low susceptibility class (27.47 %), moderate susceptibility class (28.55 %), high susceptibility class (18.68 %), and very high susceptibility

class (08.21 %). The quality of the adopted model was tested by running a ROC curve. Its AUC discriminates the robustness and performance of the retained model.

A global view on the map showed that over a quarter (26.89 %) of the study area was threatened by a high or a very high susceptibility. The chief town of Setif Province (where issues were concentrated) was surrounded by high susceptibility to the phenomenon courses. This required a particular policy especially with reference to the road network ensuring the interchange between this metropolis and the neighboring towns.

This research is a realistic approach, valid and applicable in similar environments and comparable conditions.

If the study is approved by the decision-makers of the province, it can serve as an effective information system for integrated deployment of urban centers and their networks.

If a new data becomes available, it is possible to integrate them with our model allowing the results refining.

If this research is associated with another information system handling the vulnerability of the study area to the phenomenon, it will be manageable to undertake a SM risk mapping. Finally, the database collected is a good source of information to serve other studies or other disciplines.

References

- Abul Hasanat MH, Ramachandram D, Mandava R (2010) Bayesian belief network learning algorithms for modeling contextual relationships in natural imagery: a comparative study. *Artif Intell Rev* 34(4):291–308
- Akgun A (2012) A comparison of landslide susceptibility maps produced by logistic regression, multi-criteria decision, and likelihood ratio methods: a case study at İzmir, Turkey. *Landslides* 9:93–106
- Akgun A, Kincal C, Pradhan B (2012) Application of remote sensing data and GIS for landslide risk assessment as an environmental threat to Izmir City (West Turkey). *Environ Monit Assess* 184:5453–5470
- Anbalagan R (1992) Landslide hazard assessment and zonation mapping in mountainous terrain. *Eng Geol* 32:269–277
- Ayalew L, Yamagishi H, Ugawa N (2004) Landslide susceptibility mapping using GIS based weighted linear combination, the case in Tsugawa area of Agano River, Niigata Prefecture, Japan. *Landslides* 1:73–81

- Baeza C, Corominas J (2001) Assessment of shallow landslide susceptibility by means of multivariate statistical techniques. *Earth Surf Process Landf* 26:1251–1263
- Bouhadad Y (2008) Seismic hazard assessment in Algeria: a case study of Oran region, Northwest of Algeria. The 14th World Conference on Earthquake Engineering October 12–17, 2008, Beijing, China
- Bouhadad Y, Nour A, Laouami N, Belhai D (2003) The Beni-Ourlilane-Tachouaft fault and seismotectonic aspects of the Babors region (NE of Algeria). *J Seismol* 7:79–88
- Bourenane H, Bouhadad Y, Guettouche MS, Braham M (2014) GIS-based landslide susceptibility zonation using bivariate statistical and expert approaches in the city of Constantine (NE Algeria). *Bull Eng Geol Environ*:1–19
- Chung CJF, Fabbri AG (1999) Reasoning prediction models for landslide hazard mapping. *Photogramm Eng Remote Sens* 65(12):1389–1399
- Conforti M, Aucelli PP, Robustelli G, Scarciglia F (2011) Geomorphology and GIS analysis for mapping gully erosion susceptibility in the Turbolo stream catchment (Northern Calabria, Italy). *Nat Hazards* 56(3):881–898
- Cornell CA, Van Marke EH (1969) The major influence on seismic risk. *Proceedings of the third conference on earthquake engineering. Santiago, Chile. V: A-1*, 69–93
- Demir G, Aytekin M, Akgun A (2014) Landslide susceptibility mapping by frequency ratio and logistic regression methods: an example from Niksar–Resadiye (Tokat, Turkey). *Arab J Geosci* 8:1801–1812
- Djeral L, Melbouci B (2013) Contribution to the mapping of the landslide of Aïn El Hammam (Algeria). *Adv Mater Res* 601:332–336
- Djeral L, Alimirina N, Melbouci B, Bahar R (2014) Mapping and management of landslide risk in the city of Azazga (Algeria). In: Sassa K et al. (eds.) *Landslide Science for a Safer Geoenvironment*, Vol. 2
- Domzig A (2006) Active and recent deformation and tectonosedimentary structuring of the Algerian margin underwater. PHD Thesis Bretagne occidentale, Brest University, France
- England K (2011) A GIS approach to landslide hazard management for the West Coast region, New Zealand. A thesis of Master of Science in Hazard and Disaster Management, Canterbury University, 169p
- Goovaerts P (2010) Geostatistical software. *Handbook of applied spatial analysis: software tools methods and applications*. In: Fischer MM, Getis A (eds), Springer, Berlin, pp. 129–138
- Grozavu A, Plescan S, Patriche CV, Margarint MC, Rosca B (2013) Landslide susceptibility assessment: GIS application to a complex mountainous environment, the carpathians: integrating nature and society towards sustainability. *Environ Sci Eng*:31–44
- Guadri L, Hadji R, Zahri F, Rais K (2015) The quarries edges stability in opencast mines: a case study of the Jebel Onk phosphate mine, NE Algeria. *Arab J Geosci*-D-14-01383. doi:10.1007/s12517-015-1887-3
- Guettouche MS (2013) Modeling and risk assessment of landslides using fuzzy logic. Application on the slopes of the Algerian Tell (Algeria). *Arab J Geosci* 6:3163–3173
- Guzzetti F (2005) Landslide hazard and risk assessment. Unpublished PhD Thesis. PP. 389. University of Bonn, 11/2005
- Hadji R (2013) Control of geological and climatic factors on landslides in the region of Souk Ahras and Guelma, Northeast Algerian. PhD thesis University of Badji Mokhtar-Annaba, 198 p
- Hadji R, Baghem M, Boumazbeur A, Limani Y (2012) Landslides risk mapping study and their impact on the territory of Souk Ahras Province, N-E Algeria. In: *Proceedings of the Sixth International Conference Geo-Tunis*, Tunis, 26–30 March 2012, pp. 116–125
- Hadji R, Boumazbeur A, Limani Y, Baghem M, Chouabi A (2013) Geologic, topographic and climatic controls in landslide hazard assessment using GIS modeling: a case study of Souk Ahras region, NE Algeria. *Quat Int* 302:224–237
- Hadji R, Boumazbeur A, Demdoum A, Limani Y (2014) Climate change and their influence on shrinkage-swelling clays susceptibility in a semi-arid zone: a case study of Souk Ahras Municipality, NE-Algeria. *Desalin Water Treat* 52:10–12
- Haneberg WC, Gokce AO, (1994) Rapid water-level fluctuations in a thin colluvium landslide west of Cincinnati. *U.S. Geological Survey Bulletin* 2059-C (16 p)
- Harbi A, Maouche S, Ayadi H (1999) Neotectonics and associated seismicity in the Eastern Tellian Atlas of Algeria. *J Seismol* 3:95–104
- Harbi A, Maouche S, Benhallou H (2003) Re-appraisal of seismicity and seismotectonics in the North-Eastern Algeria Part II: 20th century seismicity and seismotectonics analysis. *J Seismol* 7:221–234
- Jaupaj O, Lateltin O, Lamaj M (2014) Landslide susceptibility of Kavaja, Albania. In: *Landslide science for a safer geoenvironment*. p 351–356
- Jibson RW (1996) Use of landslides for paleoseismic analysis. *Eng Geol* 43(4):291–323
- Kamp U, Growley B, Khattak G, Ghazanfar A, Owen L (2008) GIS-based landslide susceptibility mapping for the 2005 Kashmir earthquake region. *Geomorphology* 101:631–642
- Kundu S, Saha AK, Sharma DC, Pant CC (2013) Remote sensing and GIS based landslide susceptibility assessment using binary logistic regression model: a case study in the Ganeshganga Watershed, Himalayas. *J Indian Soc Remote Sens* 41(3):697–709
- Lee S, Choi U (2003) Development of GIS-based geological hazard information system and its application for landslide analysis in Korea. *Geosci J* 7:243–252
- Mair A, Fares A (2010) Assessing rainfall data homogeneity and estimating missing records in Makaha Valley, O’ahu, Hawaii. *J Hydrol Eng* 15(1):61–66
- Malet JP, Maquaire O (2008) Risk assessment methods of landslides, RAMSOIL report 2.2. Accessible via www.ramsoil.eu
- Mastere M (2011) Mass movements susceptibility in the Chefchaouen Province (central Rif, Morocco): spatial analysis, multi-scale probabilistic modeling and impact on development and planning. PhD thesis, University of Western Brittany, 316 p
- Mastere M, Van Vliet LB, Mansour M, Aït Brahim L (2011) Spatiotemporal analysis of landslides using digital photogrammetry and DEM. *Remote Sens Rev* 10:147–156
- Mastere M, Van Vliet Lanoë B, Aït Brahim L, El Moulat M (2014) A linear indexing approach to mass movements susceptibility mapping: a case of the Chefchaouen Province (Morocco). *Revue internationale de géomatique* 05/2015; 25(2):245–265
- Ohlmacher GC, Davis JC (2003) Using multiple logistic regression and GIS technology to predict landslide hazard in northeast Kansas, USA. *Eng Geol* 69:331–343
- Pallás R, Manuel J, Marta V, Ester Falgása G, Alemana X, Muñoz AA (2004) Pragmatic approach to debris flow hazard mapping in areas affected by Hurricane Mitch: example from NW Nicaragua. *Eng Geol* 72:57–72
- Pareek N, Sharma ML, Arora MK (2010) Impact of seismic factors on landslide susceptibility zonation: a case study in part of Indian Himalayas. *Landslides* 7(2):191–201
- Parise M, Jibson WR (2000) A seismic landslide susceptibility rating of geologic units based on analysis of characteristics of landslides triggered by the 17 January, 1994 Northridge, California earthquake. *Eng Geol* 58:251–270
- Park S, Choi C, Kim B, Kim J (2013) Landslide susceptibility mapping using frequency ratio, analytic hierarchy process, logistic regression, and artificial neural network methods at the Inje area, Korea. *Environ Earth Sci* 68:1443–1464
- Phillips JD (2006) Evolutionary geomorphology: thresholds and nonlinearity in landform response to environmental change. *Hydrol Earth Syst Sci Discuss* 3(2):365–394
- Pourghasemi HR, Pradhan B, Gokceoglu C (2012) Application of fuzzy logic and analytical hierarchy process (AHP) to landslide susceptibility mapping at Haraz watershed, Iran. *Nat Hazards* 63:965–996

- Pourghasemi HR, Pradhan B, Gokceoglu C, Mohammadi M, Moradi HR (2013) Application of weights-of-evidence and certainty factor models and their comparison in landslide susceptibility mapping at Haraz watershed, Iran. *Arab J Geosci* 6:2351–2365
- Pradhan B (2013) A comparative study on the predictive ability of the decision tree, support vector machine and neuro-fuzzy models in landslide susceptibility mapping using GIS. *Comput Geosci* 51: 350–365
- Pradhan B, Lee S (2010) Landslide susceptibility assessment and factor effect analysis: back-propagation artificial neural networks and their comparison with frequency ratio and bivariate logistic regression modeling. *Environ Model Software* 25(6):747–759
- Regmi AD, Devkota KC, Yoshida K, Pradhan B, Pourghasemi HR, Kumamoto T, Akgun A (2014) Application of frequency ratio, statistical index, and weights of evidence models and their comparison in landslide susceptibility mapping in Central Nepal Himalaya. *Arab J Geosci* 7(2):725–742
- Sadigh K, Chang CY, Abrahamson NA, Chiou SJ, Power MS (1993) Specification of long period ground motion. Updated attenuation relationships for rock site conditions and adjustment factors for near fault effects. Proceedings of ATC-17-1 seminar on seismic isolation, passive energy dissipation, and active control. March 11–12 San Francisco, California, pp. 59–70
- Saunders W, Glassey P (2007). Guidelines for assessing planning, policy and consent requirements for landslide prone land. GNS Science Miscellaneous Series 7, Feb. 2007
- Schumm SA (1979) Geomorphic thresholds: the concept and its applications transactions of the Institute of British Geographers, NS4: 4, 485–515
- Schumm SA (1991) To interpret the earthen ways to be wrong. Cambridge University Press, New York
- Schumm SA, Dumont JF, Holbrook JM (2000) Active tectonics and alluvial rivers. Cambridge University Press, New York
- Sharma LP, Nilanchal P, Ghose MK, Debnath P (2013) Synergistic application of fuzzy logic and geo-informatics for landslide vulnerability zonation—a case study in Sikkim Himalayas. *India Appl Geomat* 5:271–284
- Thibault S (2011) Barycentre d'un reseau fractal, lagtime et temps de concentration. HAL Id: hal-00655526 <https://hal.archives-ouvertes.fr/hal-00655526>
- Thiery Y, Malet JP, Sterlacchini S, Puissant A, Maquaire O (2007) A landslide susceptibility assessment by bivariate methods at large scales: application to a complex mountainous environment. *Geomorphology* 92:38–59
- Varnes DJ (1978) Slope movement types and processes. In: Schuster RL, Krizek RJ (eds) Special report 176: landslides: analysis and control. Transportation and Road Research Board, National Academy of Science, Washington D. C, pp 11–33
- Varnes DJ (1984) Landslide hazard zonation: a review of principles and practice. UNESCO, France, pp 1–63
- Vila JM (1980) La chaîne alpine nord-orientale et des confins algéro-tunisiens. Thèse Doctorat, Université P. et M. Curie, Paris VI
- Wells DL, Coppersmith KJ (1994) Updated empirical relationships among magnitude, rupture length, rupture area, and surface displacement. *Bull Seismol Soc Am* 84:974–1002
- Youssef AM, Pradhan B, Tarabees E (2010) Integrated evaluation of urban development suitability based on remote sensing and GIS techniques: contribution from analytic hierarchy process. *Arab J Geosci* 4(3–4):463–473
- Zhou CH, Lee CF, Li J, Xu ZW (2002) On the spatial relationship between landslides and causative factors on Lantau Island, Hong Kong. *Geomorphology* 43:197–207